Indian Journal of Pure & Applied Physics
Vol. 61, March 2023, pp. 153-157
DOI: 10.56042/ijpap.v61i3.68621

Multi-functional Behaviour of Eu_2O_3 Embedded 3D Mesoporous Silica Template KIT-6

Sweta[a], Partha Pratim Das[b] & Shilpi Banerjee[a,c]*

[a]PG Department of Physics, Magadh University, Bodh Gaya 824 234, Bihar, India
[b]PG Department of Chemistry, Magadh University, Bodh Gaya 824 234, Bihar, India
[c]Department of Physics, Gautam Buddha Mahila College, Gaya 823 001, Bihar, India

Received 13 November 2022; accepted 13 February 2023

Rare-earth (RE) oxide embedded ordered mesoporous silica have been successfully prepared via a solution impregnation method. The structure and physical property of the nanocomposites (NCs) were studied by low-angle X-ray diffraction, Transmission Electron Microscopy (TEM), Photoluminescence (PL) and magnetic measurement. The NCs exhibited the room temperature $^5D_0 \rightarrow {}^7F_j$ transition emission due to the presence of Eu^{3+} ions. Also the NC system showed a room temperature weak ferromagnetism due to the large oxygen vacancy present in the system. Photoluminescence, magnetic property and large surface area, make these NCs ideal multi-functional materials, which will have potential applications in the field of bio-medicine and drug-delivery. These kinds of nanocomposites are promising candidates for fabrication of various environment friendly smart devices.

Keywords: Nanocomposites; Mesoporous Materials; Rare earth oxide; Magnetic Property

1 Introduction

Mesoporous magnetic nanomaterials have been extensively investigated because of their potential application in many areas including adsorption, catalysis, sensors, drug delivery, biomedical application, storage for lithium ion battery, luminescent devices, photoelectrochemical (PEC) application for water splitting and many more[1-7]. These materials were developed for biomedical applications such as magnetic targeted drug delivery, Magnetic Resonance Imaging (MRI) and separation[8-10]. Rare earth compounds have acquired a lot of importance due to their potential applications in the fields of high performance luminescent devices and catalysis[11]. The interest arose because of their useful electronic, optical and chemical properties due to the presence of 4f electrons[12,13]. Eu_2O_3 is one of the most important oxide phosphors which exhibits a luminescence spectrum centered around 612 nm corresponding to one (red) of the three primary colors (red, blue and green)[14]. Eu_2O_3 nanoparticles have been prepared by means of laser evaporation, colloidal chemistry, sol-gel method *etc*[15-17]. Also emission spectra of Eu embedded in various matrices have been investigated[18-20]. The luminescence properties of Eu^{3+} ion-doped nanomaterials and inorganic glasses have been used in the fields of displays, optical telecommunication, optoelectronic devices, lasers etc because of their sharp-monochromatic emission lines[21-23]. Luminescence property of europium has recently been used for diagnostic purpose in biomedical technology[24,25]. In recent times europium oxide nanoparticles exhibits potential application as highly efficient photoelectrodes for photo-electrochemical water splitting and photocatalyst in the degradation of biodegradable waste.[26,27]The efficiency of the europium oxides directly related to its morphology, particle size and surface area.In this work we have used a simple, facile and low-cost wet-chemical impregnation method to fabricate europium oxide loaded highly ordered mesoporous silica template KIT-6 nanocomposite. The europium oxide nanoparticles within the pore channel of 5 nm were found to exhibit photoluminescence as well as ferromagnetic-like behaviour. Also the mesoporous silica template provides highly stable microstructure to the nanocomposites along the large surface area. Such multifunctional behaviour will make this mesoporous nanocomposite as a potential candidate for fabricating systems with capabilities of magnetic drug delivery with the possibility of tracing the progress by photoluminescence characteristics[28-30] and

*Corresponding authors: (E-mail: shilpigbbanerjee@gmail.com)

many more smart devices. In this work, the details have been discussed.

2 Experimental Method

2.1 Preparation Method

The synthesis of KIT-6 powder which is the mesoporous silica template of our concern has been described earlier[31]. 1 gm of P-123 as template was dissolved in a mixture of 1.96 gm of conc. HCl (35%) and 36 gm of distilled water. The said mixture was kept on stirring for ~ 1 hour period at room temperature (308 K), followed by addition of 1 gm of butanol. Further, the resulting mixture was again kept on stirring for ~ 1h.The resulting mixture was treated with 2.15 gm of tetraethyl orthosilicate (TEOS). The Solution was further kept on stirring for 1 day at room temperature (~308 K).Resulting mixture was hydrothermally processed inside a stainless steel autoclave (Teflon-lined) for ~ 1 day at 393 K. Resulting product was filtered, followed by washing using distilled H_2O, before collection. White powder was obtained and dried (~ 24 h at ~ 333 K). After that, calcination was performed for the removal of the surfactant at 823 K for ~ 5 h. using impregnation procedure mentioned nanocomposite was synthesized. Inside a the solution of $Eu(NO_3)_3$ [Europium Nitrate]in EtOH,KIT-6 silica powder (0.5 gm) was immersed followed by stirring for ~ 24 h. Incorporated KIT-6 was filtered and collected after washing by EtOH and distilled H_2O, for several times. Resulting rinsed KIT-6 powder was kept for drying for one week at room temperature. Specimen was sintered at 873 K for 4 h.

2.2 Structural Characterization

Small angle X-ray diffraction of different samples was carried out by X-ray Diffractometer model Bruker D8 using CuK_α radiation. Using a JEOL 2010 TEM instrument, microstructures of the synthesized materials were examined. Using a Quanta chrome Autosorb-1 C at 77 K, N_2 adsorption measurements have been performed. Surface area was calculated using the BET equation. UV-Vis absorbance spectra were measured at room temperature in air using Cary 5000 UV-Vis-NIR spectrophotometer over the range from 200 to 800 nm using colloidal suspension of particles dispersed in methanol. The PL studies were performed using a FluoroMax-4 Spectrofluorometer from Horiba Jobin, which could generate tunable wavelength. MPMS Superconducting Quantum Interference Device Magnetometer was used for the study of magnetic properties in the range 2-300 K. M/S Quantum Design U.S.A. supplied the instrument.

3 Results and Discussions

TEM (Transmission Electron Micrograph) of KIT-6, our mesoporous silica template is displayed in Fig. 1(a). The estimated value of pore width of KIT-6 from TEM image was found to be around 5 nm. Fig. 1(b) gives the small angle X-Ray diffraction (SAXRD) pattern of Eu_2O_3–KIT-6 nanocomposite, which exhibits a well-resolved diffraction peak attributed to the characteristics peaks (211) of three dimensional (3D) cubic mesoporous structure of KIT-6. Low-angle region analysis of the nanocomposite exhibited characteristic reflections of high quality ordered porous structure, still preserved after the incorporation of the europium oxide inside the pores of KIT-6.This was again confirmed by the microstructure of the nanocomposite which is given in Fig. 1 (c).The latter shows that europium oxide has grown within the pores of the template. Electron diffraction pattern obtained from Fig. 1 (c) which is shown in Fig. 1 (d) is the confirmation. From Fig. 1 (d), inter planar distances were measured. These values are found to be in satisfactory agreement with the JCPDS (File No.76-0154) data for europium oxide. Table 1 summarizes these values which are

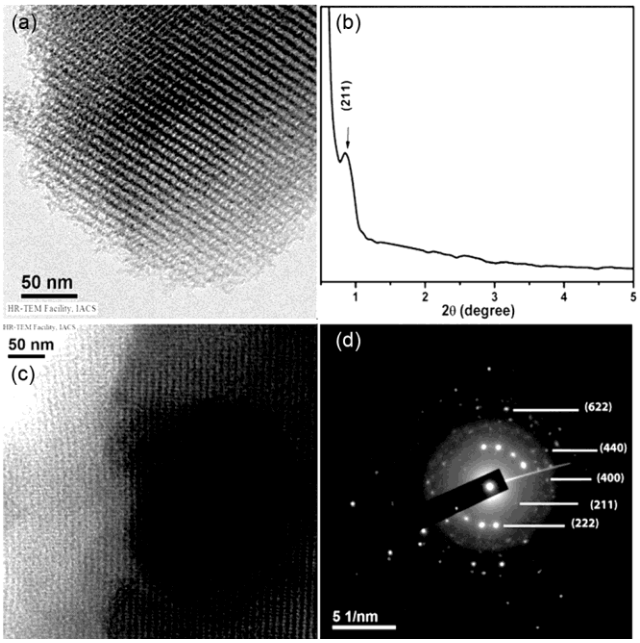

Fig. 1 — (a) Transmisson Electron Micrograph of pure KIT-6 (b) Small angle x-ray diffractogram of Eu_2O_3-KIT-6 nanocomposite (c) Transmisson Electron Micrograph of Eu_2O_3-KIT-6 nanocomposite (d) Electron Diffraction Pattern of Fig. 1(c).

Table 1 — Comparison of obtained d_{hkl} values from electron diffraction rings from Fig. 2(d) with ASTM dat

Observed d_{hkl} (nm)	ASTM data of Eu_2O_3(JCPDS no. 76-0154)(nm)	Corresponding (hkl) plane
0.445	0.442	(211)
0.310	0.312	(222)
0.269	0.271	(400)
0.191	0.191	(440)
0.165	0.163	(622)

compared with JCPDS data for europium oxide. It is evident that the europium oxide phase is sparsely distributed within the nanopores of silica. The data of EDAX measurements are summarized in Table 2. This shows the existence of a component consisting of Eu in the nanocomposite. Also it should be evident that no other element (apart from Si, O and Eu) is present in the nanocomposite. From the EDAX data the estimated amount of Eu_2O_3 was found to be 2.15 wt% in the nanocomposite.

The mesoporous structure of the KIT-6 and Eu_2O_3– KIT-6 were also confirmed by N_2 adsorption–desorption isotherms shown in Figs. 2 (a) and (b) respectively. These can be closely related to type IV isotherms which are characteristic of mesoporous materials. The BET surface area estimated for the KIT-6 is 617 m^2gm^{-1} and the pore volume is 0.9725cm^3gm^{-1}. The same corresponding to the Eu_2O_3–KIT-6 nanocomposite was 302 m^2gm^{-1} and 0.8090 cm^3gm^{-1}respectively. The specific surface area and pore volume of the KIT-6 samples is found to decrease on loading the Eu_2O_3 inside the mesopores, which confirm the incorporation of Eu_2O_3 inside the pores of KIT-6.

Considering the potential optoelectronic application of europium oxide embedded KIT-6 the optical absorbance and photoluminescence properties were studied. The results are shown in Figs. 3 (a) and (b) respectively. The UV-Vis absorption spectra showed two sharp peaks at 4.9 eV and 3.65 eV. The first peak at 4.9 eV corresponds to KIT-6[32]and the second peak around 3.65 eV is associated with Eu_2O_3[33]. It can be seen that the optical band gap of europium oxide has shifted towards high energy region compared to earlier report[33].This is ascribed to the quantum confinement effect. Fig. 3 (b) shows the room temperature photoluminescence spectra of the nanocomposite when the latter was excited at 340 nm. In the spectra four peaks are observed at 579 nm, 590 nm, 611 nm and 650 nm. For rare-earth ions the emission spectrum arises due to transitions within 4f

Table 2 — Data obtained from EDAX analysis

Element	Atomic%
O	49.19
Si	44.27
Eu	6.54

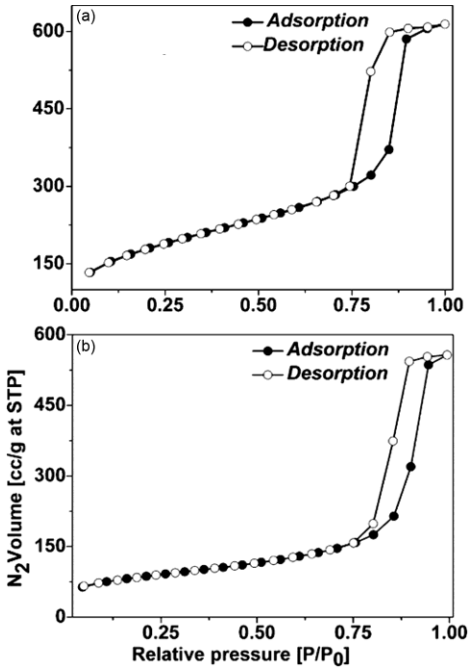

Fig. 2 — (a) and (b) N_2 adsorption/desorption isotherms of KIT-6 and Eu_2O_3-KIT-6 nanocomposite respectively.

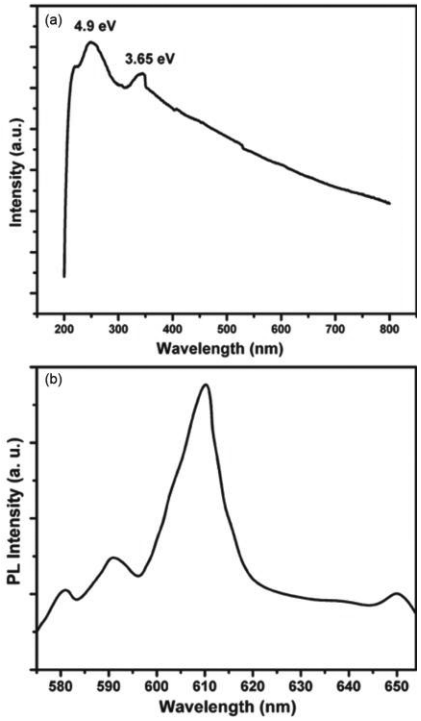

Fig. 3 — (a) UV-vis study and (b) Photoluminence spectra at room temperature of mesoporous Eu_2O_3-KIT-6 nanocomposite.

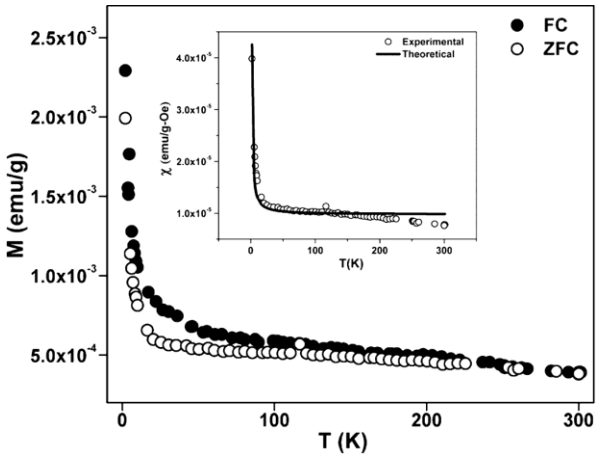

Fig. 4 — Variation of Magnetization as a function of temperature under Zero Field Cooled (ZFC) and Field Cooled (FC) situations. Inset shows experimental and theoretically fitted susceptibility vs temperature curve for Eu_2O_3-KIT-6 nanocomposite under ZFC conditions.

shell of electrons [14, 18].The emission peaks at 579 nm, 590 nm, 611nm and 650 nm correspond to the transitions ${}^5D_0 \rightarrow {}^7F_0$, ${}^5D_0 \rightarrow {}^7F_1$, ${}^5D_0 \rightarrow {}^7F_2$ and ${}^5D_0 \rightarrow {}^7F_3$ respectively. The line ${}^5D_0 \rightarrow {}^7F_1$ originates from MD (magnetic dipole allowed) transition and ${}^5D_0 \rightarrow {}^7F_2$ arises from ED (electric dipole allowed) transition**.** It is therefore evident that the nanocomposite exhibited good emission behaviour.

Figure 4 gives the variation of susceptibility (χ=M/H) as a function of temperature under zero-field cooled (ZFC) as well as field cooled (FC) situations at a field 50 of Oe. Fig. 5 (a) and (b) display the magnetization as a function of magnetic field at the temperatures 2 K and 300 K respectively. These show hysteresis loops indicating a ferromagnetic like behavior of our specimen. However, magnetization value is rather small. The absence of any magnetic phase or impurity atoms with magnetic spins was confirmed from the microstructure and the EDAX analysis. This leads us to conclude that the behaviour is intrinsic to the nanocomposite being studied here. The presence of Eu_2O_3 nanoparticles in the nanopores generates a large surface area which gives rise to an increase of surface defects (*e.g.*, oxygen vacancies) having magnetic moments. Magnetization in nanostructured oxide materials arising due to the presence of oxygen vacancies has been reported earlier[34,35]. We have fitted the χ *vs.* T curve to a two dimensional ferromagnetic model[36] using the expression

$$\chi = ae^{\left(\frac{4\pi S^2 m}{K_B T}\right)} \quad \ldots (1)$$

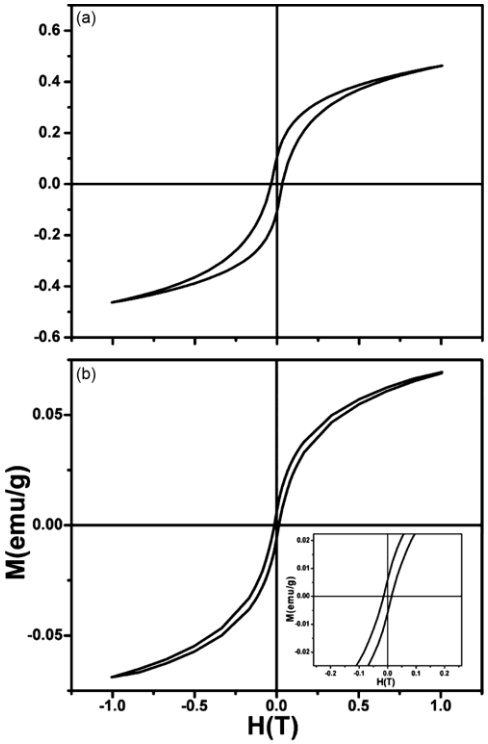

Fig. 5 — Magnetization as a function of magnetic field curve at (a) 2 K and (b) 300 K for Eu_2O_3-KIT-6 nanocomposite. Inset of (b) shows magnified view of M-H curves at 300 K.

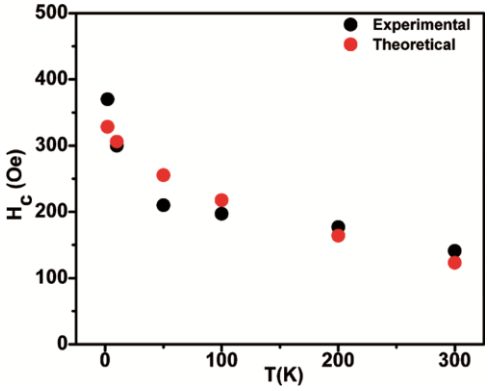

Fig. 6 — Variation of coercivity as a function of temperature for the nanocomposite.

Where "a" is a constant, S the spin quantum number, K_B the Boltzmann constant and T the temperature. S was taken as 3 (Configuration of Eu^{3+} = [Xe] $4f^6$). The results are shown in inset of Fig. 4. The fitting is found to be satisfactory. As a function of temperature, how the coercivity varies has been displayed in Fig. 6. Data have been fitted to the following equation specific for a set of ferromagnetic nanoparticles viz[37],

$$H_C = H_{CO}\left[1 - \frac{T}{T_B}\right]^{\frac{1}{2}} \quad \ldots (2)$$

Where, H_{CO} = coercivity at T = 0 K, T = temperature and T_B= the blocking temperature above which the system shows superparamagnetism. From this fitting a value of T_B = 722 K was extracted.

4 Conclusions

Prepared Eu_2O_3 embedded silica template KIT-6 having mesoporous nature, was prepared using a simple and facile impregnation method. Transmission electron diffraction studies and EDAX measurements confirmed the presence of Eu_2O_3 in the composite and absence of any other impurity phase. The optical band gap of the Eu_2O_3 in the nanocomposite increased due to quantum confinement effect. The room temperature photoluminence spectra showed four well intense emission peaks corresponding to $^5D_0 \rightarrow {}^7F_j$ (j=0, 1, 2, 3) transitions. The nanocomposite showed ferromagnetic like behaviour at room temperature which was ascribed to an increase of surface defects in Eu_2O_3.Combining the properties of photoluminence, ferromagnetism and large surface area these multifunctional nanocomposites have potential applications in the field of biomedicine, drug delivery systems, renewable energy storage systems, catalysis and sensor.

References

1 Kim J, Lee J E, Lee J, Ho Yu J, Kim B C, An K, Hwang Y, Shin C H, Park J G, Kim J & Hyeon T, *J Am Chem Soc*, 128 (2006) 688.

2 Wu Z, Yu K, Zhang S & Xie Y, *J Phys Chem C*, 114 (2010) 18753.

3 Mukherjee K & Majumder S B, *J Appl Phys*, 106 (2009) 064912.

4 Banerjee S, Hajra P, Bhaumik A & Chakravorty D, *Chem Phys Lett*, 541 (2012) 96.

5 Perkas N, Wang Y, Koltypin Y, Gedanken A & Chandrasekaran S, *Chem Commun*, (2001) 988.

6 Banerjee S, Datta A, Bhaumik A & Chakravorty D, *Bull Mater Sci*, 35 (2012) 919.

7 Zhang X, Wang F, Huang H, Li H, Han X, Liu Y& Kang Z, *Nanoscale*, 5 (2013) 2274.

8 Huang S, Fan Y, Cheng Z, Kong D, Yang P, Quan Z, Zhang C & Lin J, *J Phys Chem C*, 113 (2009) 1775.

9 Hao W, Xi Y, Hu J, Wang T, Du Y & Wang X L, *J Appl Phys*, 111 (2012) 07B301.

10 Zhang K, Amponsah O, Arslan M, Holloway T, Cao W & Pradhan A K, *J Appl Phys*, 111 (2012) 07B525.

11 Xu A W, Cao Y & Liu H Q, *J Catal*, 207 (2002) 151.

12 Yang H P, Zhang D S, Shi L Y & Fang J H, *Acta Mater*, 56 (2008) 955.

13 Fan W Q, Song S Y, Feng, Lei Y Q, Zheng G L & Zhang H J, *J Phys Chem C*, 112 (2008) 19939.

14 Silversmith A J, Boye D M, Anderman R E & Brewer K S, *J Lumin*, 94 (2001) 275.

15 Eilers H & Tissue B M, *Chem Phys Lett*, 251 (1996) 74.

16 Wakefield G, Keron H A, Dobson P J & Hutchson J L, *J Colloid Interface Sci*, 215 (1999) 179.

17 Patra A, Sominska E, Ramesh S, Koltypin Y & Zhong Z, *J Phys Chem B*, 103 (1999) 3361.

18 Mohanty P & Ram S, *J Mater Chem*, 13 (2003) 3021.

19 Reisfeld R, Zigansky E & Gaft M, *Mol Phys*, 102 (2004) 1319.

20 Babu S, Schulte A & Seal S, *Appl Phys Lett*, 92 (2008) 123112.

21 Rubinger C P L, Costa L C, Macatrão M, Peres M, Monteiro T, Costa F M, Franco N, Alves E, Saggioro B Z, Andreeta M R B & Hernandes A C, *Appl Phys Lett*, 92 (2008) 252904.

22 Maheswari D U, Kumar J S, Moorthy L R, Jang K & Jayasimhadri M, *Physica B*, 403 (2008) 1690.

23 Liu X & Lin J, *J Appl Phys*, 100 (2006) 124306.

24 Wong K L, Law G L, Murphy M B, Tanner P A, Wong W T, Lam P K S & Lam M H W, *Inorg Chem*, 47 (2008) 5190.

25 Gai S, Yang P, Wang D, Li C, Niu N, He F, Zhang M & Lin J, *RSC Adv*, 2 (2012) 3281.

26 Zeng C H, Zheng K, Lou K L, Meng X T, Yan Z Q, Ye Z N, Su R R & Zhong S, *Electrochimica Acta*, 165 (2015) 396.

27 Kaur M & Verma N K, *J Mater Sci: Mater Electron*, 24 (2013) 1121.

28 Xu Z, Cao Y, Li C, Ma P, Zhai X, Huang S, Kang X, Shang M, Yang D, Dai Y & Lin J, *J Mater Chem*, 21 (2011) 3686.

29 Tian G, Gu Z, Liu X, Zhou L, Yin W, Yan L, Jin S, Ren W, Xing G, Li S & Zhao Y, *J Phys Chem C*, 115 (2011) 23790.

30 Yang P, Quan Z, Hou Z, Li C, Kang X, Cheng Z & Lin J, *Biomaterials*, 30 (2009) 4786.

31 Zhang Z, Zuo F & Feng P, *J Mater Chem*, 20 (2010) 2206.

32 Vaishnavi T S, Haridoss P & Vijayan C, *Mater Lett*, 62 (2008) 1649.

33 Jayaraj M K &Vallabhan C P G, *Thin Solid Films*, 177 (1989) 59.

34 Kodama R H, Makhlouf S A & Berkowitz A E, *Phys Rev Lett*, 79 (1997) 1393.

35 Zhang Y C, Tang J Y & Hu X Y, *J Alloys Compd*, 462 (2008) 24.

36 Takahashi M, *Phys Rev Lett*, 58 (1987) 168.

37 Childress J R, Chien C L & Nathan M, *Appl Phys Lett*, 56 (1990) 95.